EUROPEAN TRANSACTIONS ON ELECTRICAL POWER
Euro. Trans. Electr. Power (2010)
Published online in Wiley InterScience (www.interscience.wiley.com). DOI: 10.1002/etep.475

Method for estimating core losses in switched reluctance motors

M. Torrent*,†, P. Andrada, B. Blanqué, E. Martinez, J. I. Perat and J. A. Sanchez

Department of Electrical Engineering, Escola Politècnica Superior d'Enginyeria de Vilanova i la Geltrú, Universitat Politècnica de Catalunya, Barcelona, Spain

SUMMARY

The prediction of switched reluctance motor (SRM) performance requires knowledge of core losses. However, the calculation of iron losses in SRM is especially complex first because the flux waveforms are nonsinusoidal and different parts of the magnetic circuit have different waveforms and second because they are conditioned by the type of control used. This study proposes an analytical method for calculating core losses that comprises simulation of the SRM using finite element analysis to determine the magnetization curves, and SRM modeling, which enables transient simulations with the associated electronic power converter run under different control strategies. The flux density waveforms in the different parts of the SRM are derived from the flux density waveform of the stator pole that is obtained from the transient simulation. The specific core losses (in W/kg) are separated into three parts (hysteresis losses, classical eddy current losses and excess losses) and calculated using the waveforms and time derivatives of the local flux density. The core losses for each part of the SRM's magnetic circuit can be estimated using the calculated values for specific hysteresis losses, specific classical eddy current losses and specific excess losses for each zone. Adding these individual losses yields the total core losses. The method was applied to three-phase 6/4 SRM, and the calculated results were compared with experimentally obtained measurements. Copyright © 2010 John Wiley & Sons, Ltd.

KEY WORDS: switched reluctance motors; core losses; finite element method; transient simulation

1. INTRODUCTION

The switched reluctance motor (SRM) is claiming a place in the electric motor market due to its simple and rugged construction, fault tolerance capability and high efficiency. Rating the performance of an SRM requires knowledge on different losses. However, the calculation of losses in the SRM, especially the assessment of core losses, is a very difficult task mainly due to the differences in local flux density waveforms in the different zones of the magnetic circuit. Furthermore, core losses are also conditioned by the type of control used. Several authors have proposed methods for calculating core losses. Materu and Krishnan [1] described the different magnetic flux waveforms in each part of the machine and performed a Fourier analysis to determine the losses. Hayashi and Miller [2] represented the different flux density waveforms in matrix form and calculated eddy-current losses and hysteresis losses separately using reformulated Steinmetz equations. Raulin *et al*. [3] calculated core losses based on magnetic flux waveforms predicted from the motor simulation. Chindurza *et al*. [4] further pursued SRM simulation to obtain the losses from the energy cycle. Charton *et al*. [5,6] included core losses in their SRM model by using dynamic simulations. Faiz *et al*. [7] simulated the motor using finite elements methods and then calculated the losses based on the modified Steinmetz equation. Reinert *et al*. [8] also used a modified Steinmetz equation in which the remagnetization frequency is replaced with

*Correspondence to: M. Torrent, Department of Electrical Engineering, Escola Politècnica Superior d'Enginyeria de Vilanova i la Geltrú, Universitat Politècnica de Catalunya, Barcelona, Spain.
†E-mail: mtorrent@ee.upc.edu

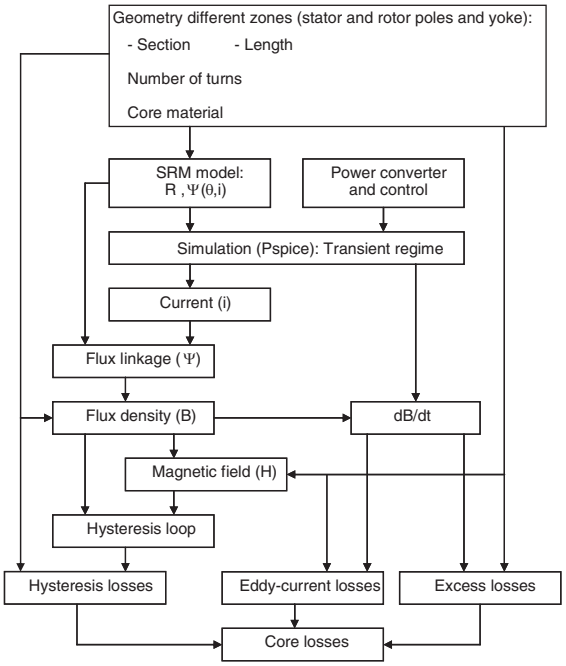

Figure 1. Flowchart of core losses calculation process.

an equivalent frequency calculated from the average remagnetization ratio. In this paper a new method for predicting core losses in SRM is presented. It takes into account the type of control used and the fact that flux waveforms in the SRM are not sinusoidal and are different in each part of its magnetic circuit. The method reported here comprises the simulation of the SRM using finite element analysis, to determine the magnetization curves, and SRM modeling, which enables transient simulations with the associated electronic power converter run under different control strategies. The core losses are separated into three parts: hysteresis losses, classical eddy current losses and excess losses. Firstly, the local hysteresis losses (in W/kg) are quantified according to the area of the hysteresis loop for each SRM zone depending on the local flux density. Secondly, the changes in local transient flux density over time and the corresponding derivative function (with respect to time) are determined for each zone. Their root mean square (rms) values are calculated and then used to determine the classical eddy-current specific losses and the excess loss (in W/kg). Lastly, the weight for each zone is calculated based on the geometric dimensions and the density of the ferromagnetic material. Using these values for specific losses and weight, one can estimate the core losses for each zone. Summing these individual losses yields the total core losses. A flowchart of the core losses calculation process is shown in Figure 1.

The method reported here was applied to a three-phase 6/4 SRM and then validated by comparing the calculated losses with experimentally measured losses. The paper is organized as follows: Section 2 presents the SRM nonlinear model; Section 3 describes the different flux density waveforms; Section 4 details how hysteresis losses and eddy current loses are computed; Section 5 shows the simulation results obtained applying the proposed method; Section 6 describes the experimental validation; and Section 7 presents the conclusions drawn from this research.

2. SRM NONLINEAR MODEL

SRM is a doubly salient pole rotational device with single excitation that usually works strongly saturated. The torque is produced by the tendency of its rotor to move to a position where

DOI: 10.1002/etep

the inductance of the excited phase winding is maximized. Therefore, a power converter with solid state interrupters is needed to generate the right sequence of phase commutation according to the position of the rotor. The behavior of the SRM drive is governed by the following phase equations [9,10]:

$$v(t) = Ri(t) + \frac{\mathrm{d}\psi(\theta, i)}{\mathrm{d}t} \tag{1}$$

$$W'(\theta, i) = \int_0^i \psi(\theta, i)\mathrm{d}i \tag{2}$$

$$T = \sum_{i=1}^{m} \left[\frac{\partial W'(\theta, i)}{\partial \theta}\right]_{i=\text{constant}} \tag{3}$$

$$J\frac{\mathrm{d}\omega}{\mathrm{d}t} = T - T_{\mathrm{L}} \tag{4}$$

where v is the voltage, i is the current, R is the resistance, ψ is the flux linkage, θ is the position, W' is the coenergy, J is the moment of inertia, ω is the angular speed, T is the motor torque, T_{L} is the load torque; and m is the number of phases.

The curves representing flux linkage with respect to current and rotor position, ψ (θ, i), called magnetization curves, are a key point for the SRM. Due to the combined effects of saturation, saliency and hysteresis, these curves are very difficult to determine with any degree of precision by means of relationships derived from SRM geometry. Their accurate determination requires finite element (FE) calculations. They are usually represented for the flux linkage according to the current at different rotor positions but they may also be represented for the flux linkage according to different positions at different currents. Modeling of SRM requires an analytical expression for magnetization curves that fits the curves obtained by FE analysis as well as possible. In this paper, the flux linkage versus position for different values of current is determined by the following equation [11]:

$$\psi(\theta, i) = p_0 + \sum_{n=1}^{n=5} p_n \cos\left(nN_{\mathrm{r}}\theta\right) \tag{5}$$

where N_{r} is the number of rotor poles and the coefficients p_0 and p_{n} are current functions obtained from (6) and (7), respectively:

$$p_0 = p_{01}i^3 + p_{02}i^2 + p_{03}i \tag{6}$$

$$p_n = p_{n1}i^3 + p_{n2}i^2 + p_{n3}i \tag{7}$$

Once the magnetization curves have been fitted, the SRM drive including the power converter and control can be simulated. Transient simulations were performed on the model using Pspice, incorporating the classical or asymmetric power converter shown in Figure 2, used under different

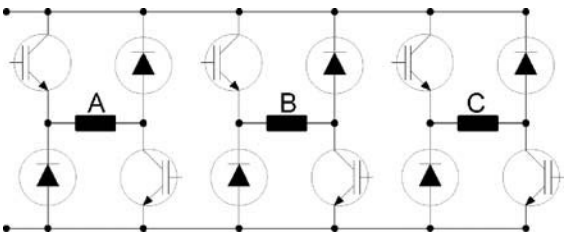

Figure 2. Classical electronic power converter (A, B, and C = motor phases).

DOI: 10.1002/etep

control strategies: constant current (hysteresis control) up to base speed and a single-pulse control for higher speeds.

3. SRM FLUX DENSITY WAVEFORMS

In the SRM, the flux density waveforms are nonsinusoidal and different parts of the magnetic circuit have different waveforms. The flux densities in the different parts of the SRM are derived from the flux density of the stator poles. Flux density waveforms of the stator poles are more or less unipolar triangular pulses and depend on the phase switch conducting period, the diode conducting period and, of course, the type of control. The flux densities of all stator phases have the same waveform, albeit shifted by the delay angle, ε, between phases ($m =$ number of phases; $N_r =$ number of rotor poles):

$$\varepsilon = \frac{2\pi}{mN_r} \tag{8}$$

The different flux waveforms in the stator yoke are obtained by summing the stator pole flux waveforms in the different zones of the magnetic circuit. The flux polarity in the rotor reverses at every half a revolution, so the rotor poles flux waveforms are bipolar. The rotor yoke flux waveform is obtained by subtracting the rotor pole flux waveforms [1,11].

There are 9 different zones in a three-phase 6/4 SRM, shown in Figure 3 [10]. Zone 1, 1′, and 1″ corresponds to the stator poles; zones 2, 3, and 3′ to the stator yoke; Zone 4 and 4′ to the rotor poles; and Zone 5 to the rotor yoke.The frequency in the different flux density waveforms is directly related to the base frequency (f_{base}) of the SRM, which corresponds to the motor's phase current:

$$f_{\text{base}} = \frac{nN_{\text{r}}}{60} \tag{9}$$

where f_{base} is measured in Hz, n is the speed in rpm, and N_{r} is the number of rotor poles.

The frequency (f) in each zone is calculated using the formulas that are collected in Table I. Although the changes in flux density over time at some of these zones are not identical (1, 1′, and 1″; 3 and 3′; 4 and 4′), they have the same frequency. For the purpose of calculating core losses, these zones can be treated as a single zone.

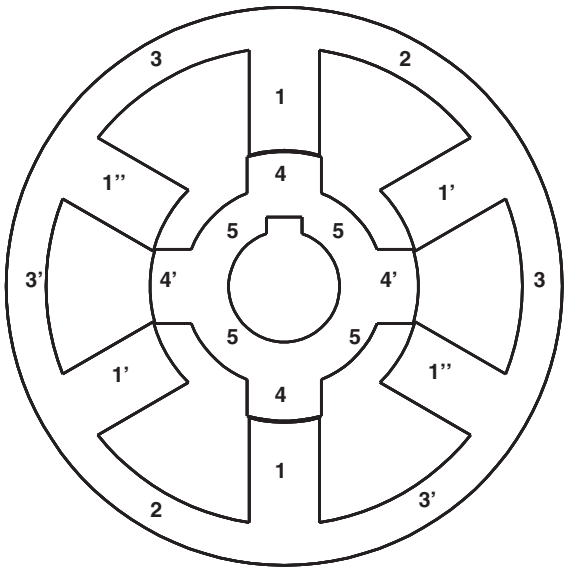

Figure 3. Zones considered for analyzing local flux density values in the 6/4 SRM studied.

DOI: 10.1002/etep

Table I. Frequency in the different parts of the magnetic core.

Zone	Frequency
Zone 1, 1′ and 1″ (stator poles)	$f=f_{\text{base}}$
Zone 2 (stator yoke)	$f=f_{\text{base}} \times m$
Zone 3 and 3′ (stator yoke)	$f=f_{\text{base}}$
Zone 4 and 4′ (rotor poles)	$f=f_{\text{base}}/N_{\text{r}}$
Zone 5 (rotor yoke)	$f=f_{\text{base}}/N_{\text{r}}$

4. CALCULATING CORE LOSSES

The calculations for core losses are based on the transient simulation performed using the aforementioned nonlinear SRM model, which incorporates values for parameters of the SRM's geometry and core material and considers different control strategies. The specific core losses (in W/kg) at every zone of the stator and rotor core (i) are then calculated using the local flux density and its time derivative. The specific core losses are divided into three parts: hysteresis losses ($P_{\text{hys},i}$), classical eddy current losses ($P_{\text{eddy},i}$), and excess losses ($P_{\text{exc},i}$). The weight for each zone (G_i) is calculated based on the geometric dimensions and the density of the ferromagnetic material. Therefore, the total core losses (P_{core}) for the different zones considered are given by the following expression:

$$P_{core} = \sum_{i}^{n} \left(P_{hys,i} + P_{eddy,i} + P_{exc,i}\right) G_i \tag{10}$$

4.1. Hysteresis losses

Hysteresis losses result from changes in the flux density (B) and magnetic field (H) of the core, which are factors that determine the area of the hysteresis loop. Therefore, quantifying hysteresis losses requires knowledge on the ferromagnetic material of the core, namely for use in constructing the hysteresis loop for each operating point. A loop should be obtained for each zone of the core, and the area under the B–H curve has to be measured. Therefore, specific hysteresis losses (P_{hys}) can be calculated using the following expression in W/kg:

$$P_{hys} = \frac{Sf}{\delta} \tag{11}$$

where S is the area under the B–H curve, f is the frequency (in Hz) for each zone; and δ is the density of the ferromagnetic material (in kg/m^3). Frequently, the specific hysteresis loops has been computed using Steinmetz equation in its original form or with some variations, usually in the exponent of the peak value of the flux density [7,8]. Recently, various authors have used Preisach-type hysteresis operators to calculate specific hysteresis losses [5]. In this paper, hysteresis loops were obtained using the relatively unknown model proposed by Leplus [12] (see Appendix).

4.2. Classical eddy-current losses

Classical eddy-current losses are produced by circulation of parasitic currents through the core. Instantaneous classical eddy-current losses ($P_{\text{eddy}}(t)$) are dictated by changes in flux density over time ($\text{d}B(t)/\text{d}t$) and can be calculated in W/kg using:

$$P_{\text{eddy}}(t) = k_{\text{eddy}} \left(\frac{\text{d}B(t)}{\text{d}t}\right)^2 \tag{12}$$

where k_{eddy} is the classical eddy current coefficient, which is usually determined by the formula [3,4]:

$$k_{eddy} = \frac{e^2}{12\rho_{fe}\delta} \tag{13}$$

DOI: 10.1002/etep

where δ is the density of the ferromagnetic material (in kg/m^3), e is the sheet thickness (in m) and ρ_{fe} is the electrical resistivity of the ferromagnetic material (in Ωm). Nevertheless, in this paper k_{eddy} is calculated using:

$$k_{eddy} = \frac{e^2}{4k_{cir}\rho_{fe}\delta} \tag{14}$$

where k_{cir} is a constant ($1 < k_{\text{cir}} < 3$) introduced to account for the fact that paths in the interior of the lamination will have smaller emf's than those near the surface [13]. Therefore the expression for the average classical eddy-current losses (P_{eddy}) in W/kg is:

$$P_{eddy} = \frac{1}{T}\int_0^T P_{eddy}(t)dt = \frac{e^2}{4k_{cir}\rho_{Fe}\delta}\frac{1}{T}\int_0^T \left(\frac{dB(t)}{dt}\right)^2 dt = \frac{e^2}{4k_{cir}\rho_{fe}\delta}\left(\frac{dB(t)}{dt}\right)^2_{rms} \tag{15}$$

4.3. Excess losses

The specific excess losses are caused by the movement of the magnetic-domain walls and domain rotation damped by eddy currents. Fiorillo and Novikov [14] proposed to calculate the instantaneous specific excess losses ($P_{\text{exc}}(t)$) by means of the following equation:

$$P_{\text{exc}}(t) = k_{\text{exc}}\left(\frac{\text{d}B(t)}{\text{d}t}\right)^{3/2} \tag{16}$$

where k_{exc} is the excess loss coefficient that is determined by curve fitting measured variations of loss with flux density and frequency. The expression for the average specific excess losses (in W/kg) is:

$$P_{\text{exc}} = \frac{1}{T}\int_0^T P_{\text{exc}}(t)\text{d}t = k_{\text{exc}}\frac{1}{T}\int_0^T \left(\frac{\text{d}B(t)}{\text{d}t}\right)^{3/2}\text{d}t = k_{\text{exc}}\left(\frac{\text{d}B(t)}{\text{d}t}\right)^{3/2}_{\text{rms}} \tag{17}$$

5. APPLYING THE PROPOSED METHOD ON A THREE-PHASE 6/4 SRM

The method reported was tested on a three-phase 6/4 SRM (voltage: 300 V; power: 750 W; and speed base: 3000 rpm). All the simulations, curves and results presented here refer to this motor, whose dimensions are indicated in Table II [7,8].

Table II. Main data of the 6/4 SRM.

Stator outer diameter	125.10 mm
Stator inner diameter	61 mm
Stack length	61 mm
Rotor diameter	60.40 mm
Rotor yoke diameter	45 mm
Air-gap	0.30 mm
Stator pole arc	30°
Rotor pole arc	32°
Stator pole width	15.79 mm
Rotor pole width	16.65 mm
Stator yoke width	9 mm
Rotor yoke width	10 mm
Shaft diameter	25 mm
Number of turns per pole	156

DOI: 10.1002/etep

5.1. Model and simulations

Figure 4 shows the finite element analysis in the aligned and unaligned positions. Figure 5 shows the results of adjusting the magnetization curves for the 6/4 SRM, in which the current interval of the curves is 1A.

Figure 6 shows plots comparing the results from the simulations to the experimental measurements for each control strategy. Generally single pulse control is used for speeds above motor base speed and constant-current control, which is implemented using PWM or hysteresis control, for speeds bellow motor base speed [11].

5.2. Flux density waveforms

The changes in current over time for each phase of the motor depend on the conduction starting time, the interval of conduction and the control type adopted [8]. For the case of a conduction interval equal to the step angle, a starting time coincident with the non-aligned position, and operation under single-pulse control, the waveform of the phase current follows the pattern shown in Figure 7 (obtained from simulation at a speed of 3000 rpm). Based on this current and on the stator and rotor core materials and geometry, the flux density waveforms for each zone were obtained through simulation (see Figure 8).

5.3. The hysteresis loops

In the SRM studied, the stator and rotor core were built using a steel sheet (FeV 600-50 HA) with the following characteristics: density 7800 kg/m^3; sheet thickness 0.5 mm; and electrical

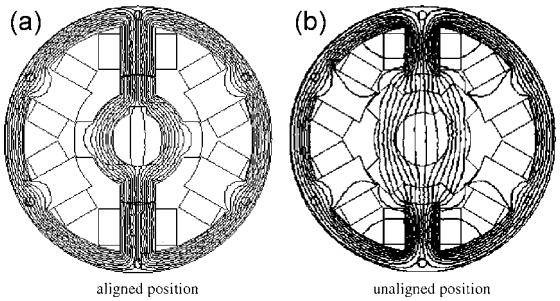

Figure 4. Finite element analysis of the 6/4 SRM. (a) Aligned position and (b) unaligned position.

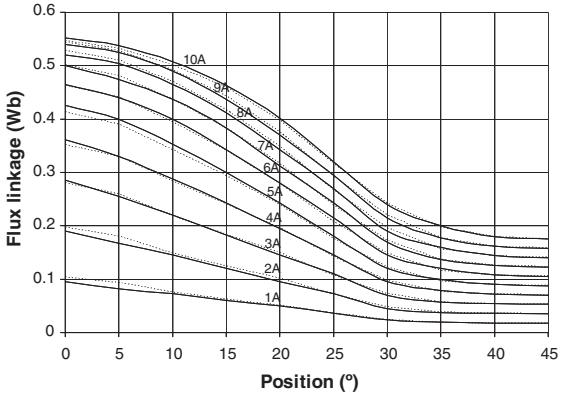

Figure 5. Comparison between experimental values (solid lines) and adjusted values (dotted lines) in the magnetization curves obtained for the 6/4 SRM (current interval = 1 A).

DOI: 10.1002/etep

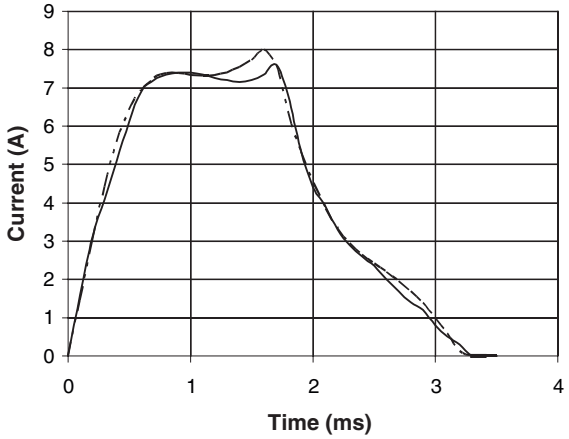

(a) Single-pulse control (3100 rpm)

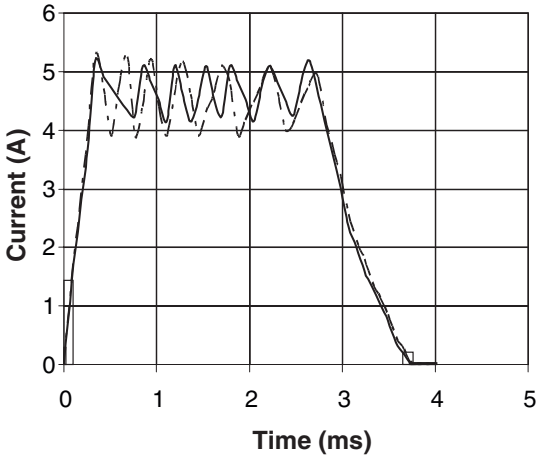

(b) Constant-current control (1850 rpm)

Figure 6. Comparison between simulation results (dotted lines) and experimental measurements (solid lines) for the 6/4 SRM. (a) Single-pulse control (3100 rpm) and (b) constant-current control (1850 rpm).

resistivity $40 \times 10^{-8}\,\Omega$m. Figure 9 shows the hysteresis loops obtained by means of the aforementioned Leplus model for each zone, using single-pulse operation at a speed of 3000 rpm. The cycle corresponding to zone 2 (stator yoke) has not been included because its area is very small.

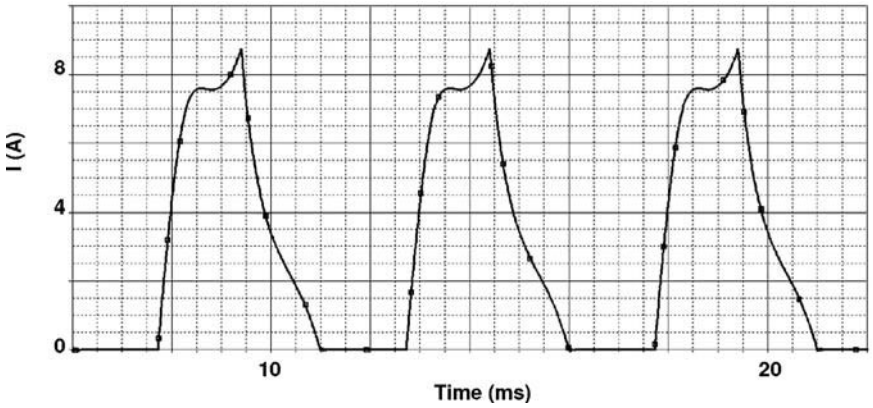

Figure 7. Phase current from simulation of the 6/4 SRM at 3000 rpm under single-pulse control.

DOI: 10.1002/etep

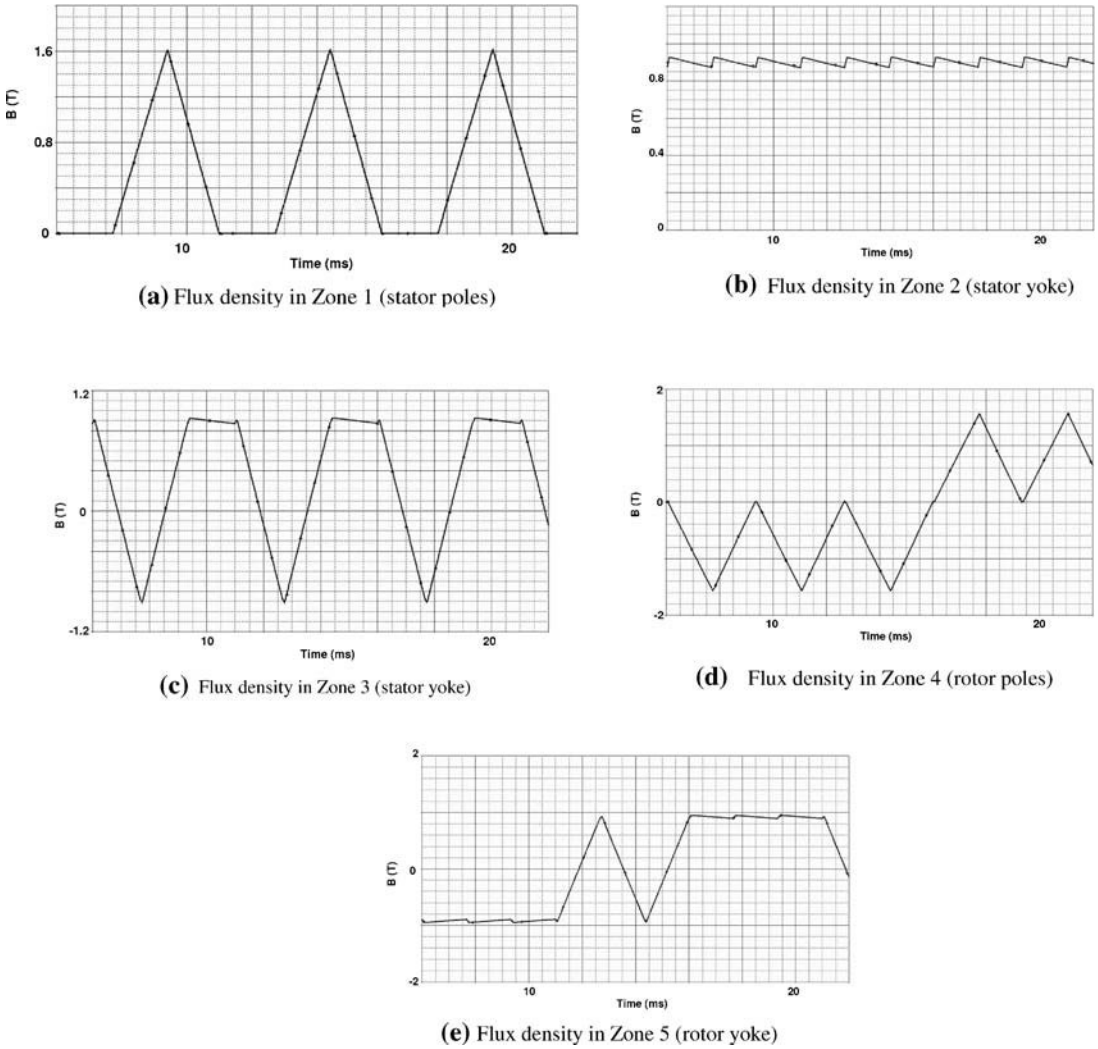

Figure 8. Local flux density values from simulation of the 6/4 SRM at 3000 rpm under single-pulse control. (a) Flux density in Zone 1 (stator poles), (b) flux density in Zone 2 (stator yoke), (c) flux density in Zone 3 (stator yoke), (d) flux density in Zone 4 (rotor poles), and (e) flux density in Zone 5 (rotor yoke).

5.4. dB(t)/dt variations

The plots in Figure 10 show the variation in d$B(t)$/dt over time for each zone and their rms values (dotted line).

5.5. Core losses results

Using the procedure described above, the core losses (in W/kg) were calculated for the SRM. Figure 11 shows the results obtained under single-pulse control, and Figure 12 shows those obtained under constant-current control.

It was observed that under single-pulse control, both hysteresis losses and eddy-current losses remain fairly constant at different speeds. Hysteresis losses are greatest in zones 4 and 5 (the rotor), whereas specific eddy-current losses are greater in zone 3 (the stator yoke). In contrast, under constant-current control, the two types of losses increase proportionally with speed, and both are greatest in zones 4 and 5 (the rotor) and in zone 3 (the stator yoke).

DOI: 10.1002/etep

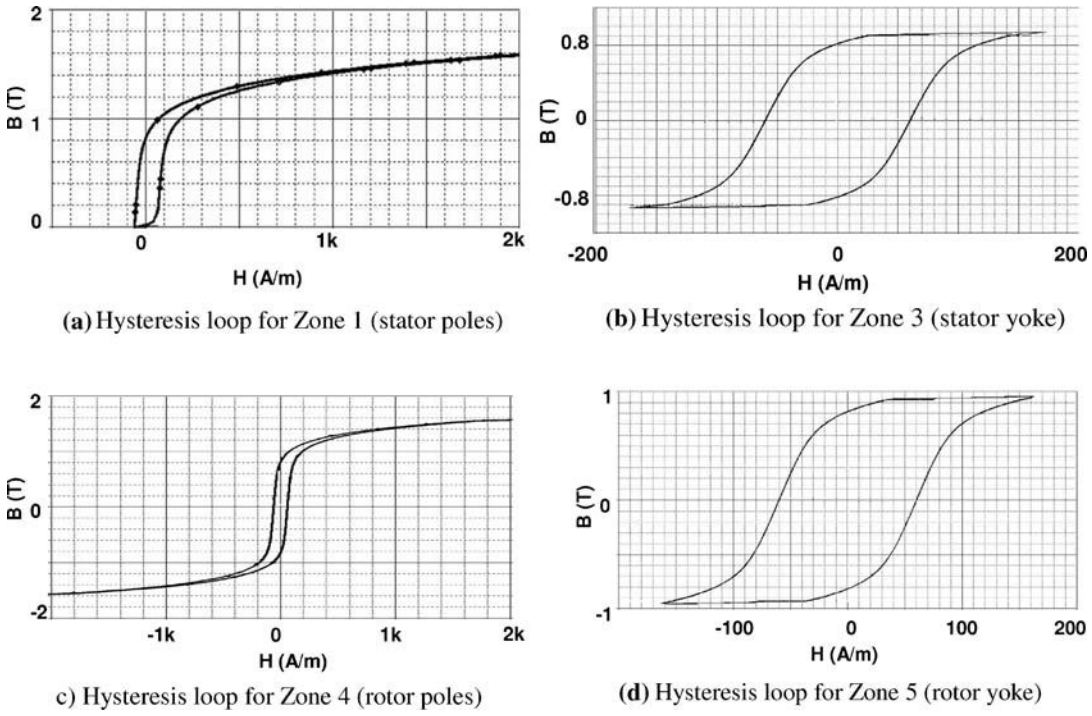

Figure 9. Local hysteresis loops from simulation of the 6/4 SRM under single-pulse control (3000 rpm). (a) Hysteresis loop for Zone 1 (stator poles), (b) hysteresis loop for Zone 3 (stator yoke), (c) hysteresis loop for Zone 4 (rotor poles), and (d) hysteresis loop for Zone 5 (rotor yoke).

6. EXPERIMENTAL RESULTS

To evaluate the proposed method an experimental setup was used (Figure 13). Core losses were determined experimentally as follows. First, a load test was used to measure the torque and speed, and thereby calculate the mechanical power output. The electrical input power was then measured, and the

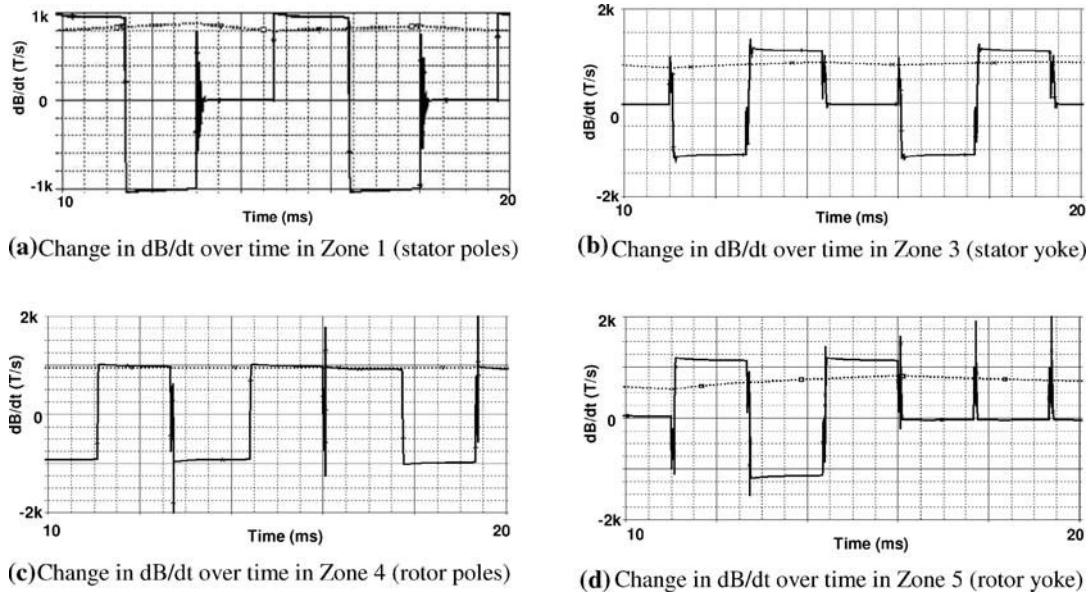

Figure 10. Local changes in dB/dt over time obtained from simulation of the 6/4 SRM under single-pulse control (3000 rpm). The dotted lines correspond to RMS values. (a) Change in dB/dt over time in Zone 1 (stator poles), (b) change in dB/dt over time in Zone 3 (stator yoke), (c) change in dB/dt over time in Zone 4 (rotor poles), and (d) change in dB/dt over time in Zone 5 (rotor yoke).

DOI: 10.1002/etep

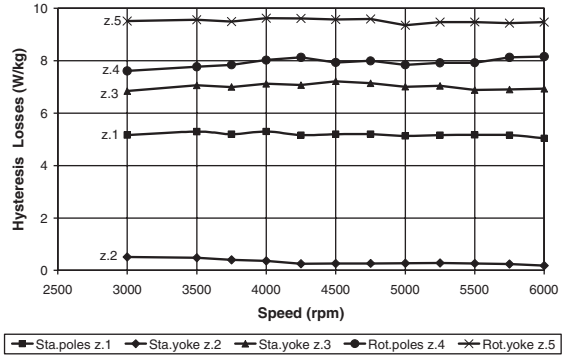

(a) Hysteresis losses

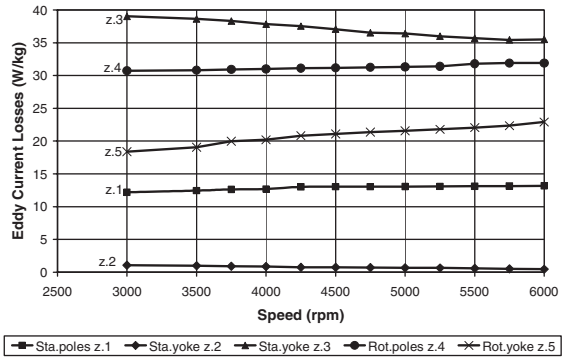

(b) Eddy-current losses

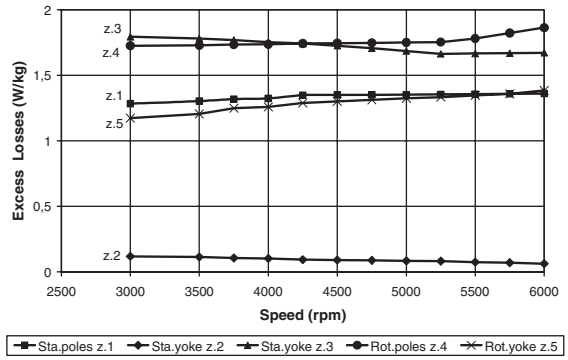

(c) Excess losses

Figure 11. Core losses in different zones of the 6/4 SRM under single-pulse control. (a) Hysteresis losses, (b) Eddy-current losses, and (c) excess losses.

efficiency and total losses were determined. Second, the resistance of the motor coils was measured at the operating temperature of the load test. The copper losses were calculated from the resistance and the current, rms values, measured at different operating points. Third, mechanical losses were obtained with the help of a conventional DC motor of known parameter values (180 V, 1.31 kW), which is similar in power to the SRM. No-load motor tests were performed on the DC motor at different speeds and the input power was measured at each test point. The two machines were then coupled mechanically, and the same test was repeated to measure the resulting input power. The difference between the two input powers, from which the copper losses in the DC motor were subtracted, corresponds to the mechanical losses of the SRM. Finally, the core losses (P_{fe}) were determined by subtracting the copper losses (P_{j}) and the mechanical losses (P_{m}) from the total losses (P_{t}):

$$P_{\mathrm{fe}} = P_{\mathrm{t}} - P_{\mathrm{j}} - P_{\mathrm{m}} \tag{18}$$

DOI: 10.1002/etep

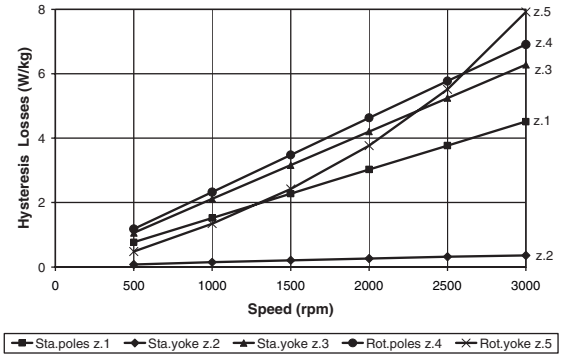

(a) Hysteresis losses

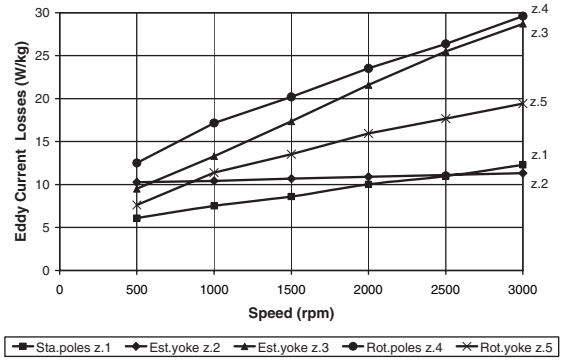

(b) Eddy-current losses

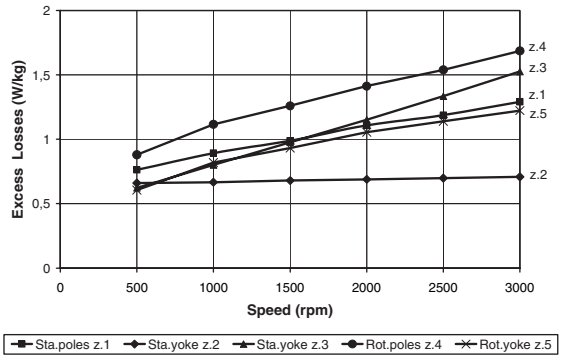

(c) Excess losses

Figure 12. Core losses in different zones of the 6/4 SRM under constant-current control. (a) Hysteresis losses, (b) eddy-current losses, and (c) excess losses.

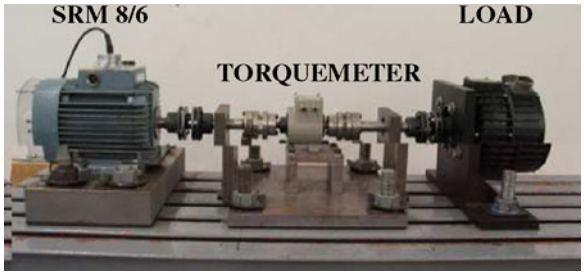

Figure 13. Experimental setup.

DOI: 10.1002/etep

Figures 14 and 15 show the breakdown of the measured losses for the SRM under single-pulse control and constant-current control, respectively.

As observed in Figures 16 and 17, the results obtained from the method described here were satisfactorily close to the measurements obtained experimentally. Moreover, the measured core losses are slightly greater than the calculated ones, which is probably due to the fact that experimental measurements account for stray load losses and rotational core losses [15], neither of which are included in the calculation method.

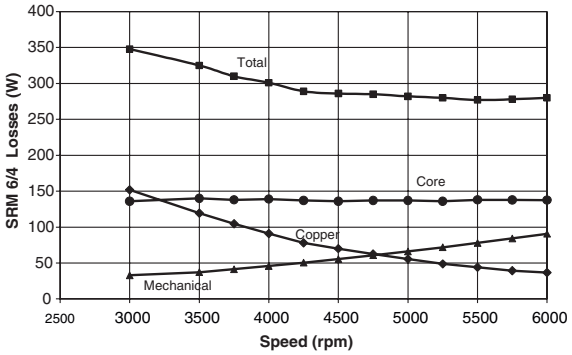

Figure 14. Separation of measured losses for the SRM under single-pulse control.

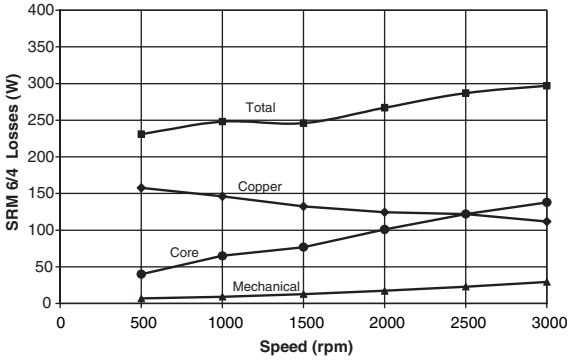

Figure 15. Separation of measured losses for the SRM under constant-current control.

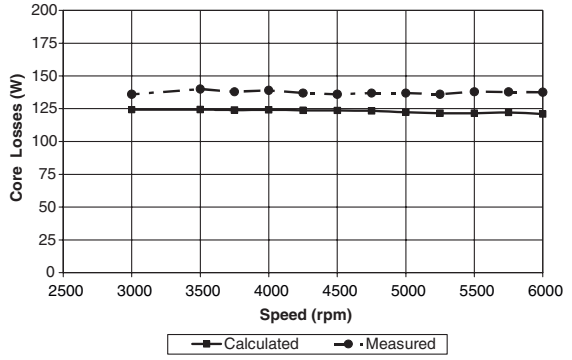

Figure 16. Calculated losses and measured losses for the SRM under single-pulse control.

DOI: 10.1002/etep

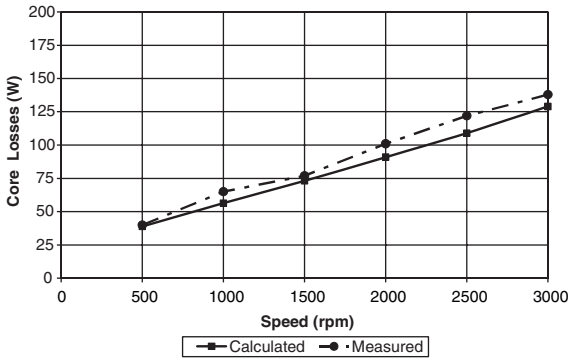

Figure 17. Calculated losses and measured losses for the SRM under constant-current control.

7. CONCLUSIONS

A new method for estimating core losses in SRM has been presented. The proposed method takes into account the type of control used and the facts that flux waveforms in the SRM are not sinusoidal and are different in each part of its magnetic circuit. The method was used to predict the iron losses in 6/4 three phases 6/4 SRM and was then validated by comparing the calculated losses to experimentally measured losses. Some differences between measured and predicted values were observed. This is attributed to the fact that stray load losses and rotational core losses were neglected in the calculation method. The method proposed here gives a detailed analysis of the losses in the different parts of the motor and can be useful for predicting losses in the design process of an SRM drive.

REFERENCES

1. Materu PN, Krishnan R. Estimation of switched reluctance motor losses. *IEEE Transactions on Industry Applications* 1992; **28**(3):668–679.
2. Hayashi Y, Miller TJE. A new approach to calculating core losses in the SRM. *IEEE Transactions on Industry Applications* 1995; **31**(5):1039–1045.
3. Raulin V, Radun A, Husain I. Modeling of losses in switched reluctance machines. *IEEE Transactions on Industry Applications* 2004; **40**(6):1560–1564.
4. Chindurza I, Dorrell DG, Cossar C. Assessing the core losses in switched reluctance machines. *IEEE Transactions on Magnetics* 2005; **41**(10):3907–3909.
5. Charton JT, Corda J, Stephenson JM, McClelland ML. Modelling and prediction of iron loss with complex flux waveforms. *IEE Proceedings—Electric Power Applications* 2005; **152**(3):862–870.
6. Charton JT, Corda J, Stephenson JM, Randall SP. Dynamic modelling of switched reluctance machines with iron losses and phase interactions. *IEE Proceedings—Electric Power Applications* 2006; **153**(3):327–336.
7. Faiz J, Ganji B, Carstensen CE, De Doncker RW. Loss prediction in switched reluctance motors using finite element method. *European Transactions on Electrical Power* 2008; **19**(5): 731–748.
8. Reinert J, Brockmeyer A, De Doncker RWAA. Calculations of losses in ferro and ferromagnetic materials based on the modified Steinmetz equation. *IEEE Transactions on Industry Applications* 2001; **37**(5):1055–1061.
9. Miller TJE, McGilp M. Nonlinear theory of the switched reluctance motor for rapid computer-aided design. *IEE Proceedings—Electric Power Applications* 1990; **37**(6):337–347.
10. Krishnan R. *Switched Reluctance Motor Drives: Modeling, Simulation, Analysis, Design and Applications*. CRC Press LLC: New York, 2001.
11. Torrent M, Andrada P, Blanqué B, Perat JI. *Simulation of Switched Reluctance Motor (SRM) Using Non-Linear Models*. Brugge: ICEM, 2002.
12. Leplus F. Bobine à noyau de fer en régime variable. Techniques de l'Ingénieur, Traité Génie électrique. D3040, 2007.
13. Slemon GR, Straughen A. *Electric Machines*. Addison-Wesley Publishing Company: 1980.
14. Fiorillo F, Novikov A. An improved approach to power losses in magnetic laminations under nonsinusoidal induction waveform. *IEEE Transactions on Magnetics* 1990; **26**(5):2904–2910.
15. Zhu G, Ramsden VS. Improved formulations for rotational core losses in rotating electrical machines. *IEEE Transactions on Magnetics* 1998; **34**(4):2234–2242.

DOI: 10.1002/etep

APPENDIX

In the model proposed by Leplus, the hysteresis loop (Figure 18) is divided into five sections, according to certain conditions that have to be accomplished by the flux density and its time derivative. Each of these sections is represented by a polynomial expression, as can be seen in the following equations.

$$\text{Section 1}: \; H = -a_1 + a_2 B + a_3 B^3 + a_4 (B + a_5)^7 \tag{19}$$

$$\text{Section 2}: \; H = a_1 + a_2 B + a_3 B^3 + a_4 (B - a_5)^7 \tag{20}$$

$$\text{Section 3}: \; H = a_6 B^7 \tag{21}$$

$$\text{Section 1b}: \; H = -a_1 + a_2\left(\frac{B + B_{\text{sat}}}{a_0} - B_{\text{sat}}\right) + a_3\left(\frac{B + B_{\text{sat}}}{a_0} - B_{\text{sat}}\right)^3 + a_4\left(\frac{B + B_{\text{sat}}}{a_0} - B_{\text{sat}} + a_5\right)^7 \tag{22}$$

$$\text{Section 2b}: \; H = a_1 + a_2\left(\frac{B - B_{\text{sat}}}{a_0} + B_{\text{sat}}\right) + a_3\left(\frac{B - B_{\text{sat}}}{a_0} + B_{\text{sat}}\right)^3 + a_4\left(\frac{B - B_{\text{sat}}}{a_0} + B_{\text{sat}} - a_5\right)^7 \tag{23}$$

with H is the magnetic field, B is the flux density, a_0, a_1, a_2, a_3, a_4, a_5, B_{sat} are the ferromagnetic material parameters.

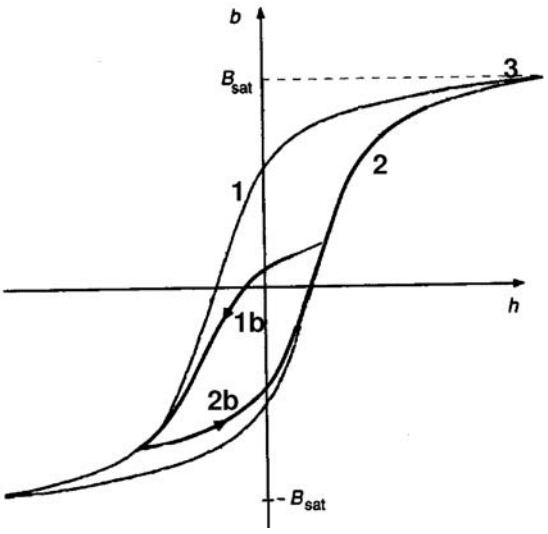

Figure 18. Hysteresis sections showing the different sections considered in the Leplus model.

DOI: 10.1002/etep